# Analysis of current and shot noise correlations in a double quantum dot interferometer with interdot spin interactions

Marko Zivkovic, Brandon W. Langley, Ivana Djuric, and Chris P. Search

# Analysis of current and shot noise correlations in a double quantum dot interferometer with inter-dot spin interactions

Marko Zivkovic, Brandon W. Langley, Ivana Djuric, and Chris P. Search

*Department of Physics and Engineering Physics,*
*Stevens Institute of Technology, Castle Point on Hudson, Hoboken, NJ 07030*

We examine an electron Aharonov-Bohm (AB) interferometer with individual quantum dots connected in parallel to macroscopic leads. Here, we focus on the effect that both inter-dot spin-spin exchange interactions and intra-dot spin flips have on the current and frequency dependent current shot noise. By appropriate control of AB magnetic flux, inter-dot Coulomb repulsion, intra-dot spin flips, and inter-dot spin-spin coupling, the probability amplitudes for the different paths of the interferometer can be controlled leading to broad tunability of both the shape and contrast of interference fringes in the current. We also show that in the shot noise at finite frequencies corresponding to the spin-spin interaction energies the noise shows pronounced super-Poissonian and sub-Poissonian structure. AB flux, which is not an integer multiple of $2\pi$, dramatically suppresses the correlations in the shot noise.

PACS numbers: 73.63.Kv,73.23Hk

## I. INTRODUCTION

The analysis of shot noise in mesoscopic circuits[1] has became an important topic in transport since it is a direct measure of interparticle correlations and therefore indicates additional information about processes in the circuit that cannot be obtained directly from standard conductance measurements such as Coulomb interactions, quantum statistics of charge carriers, available transport channels, entanglement, etc...Such effects cause the shot noise to differ from the "classical" Poissonian noise for uncorrelated transport of discrete charge carriers by leading either to a bunching in the arrival times of charge carriers (super-Poissonian statistics) or anti-bunching (sub-Poissonian statistics). Moreover, while the DC (zero frequency) shot noise measures the long time steady state correlations in the arrival times of the charge carriers, measurement of the shot noise at non-zero frequencies provides a method to measure correlations over finite time intervals, which reveal the time scales of dynamical processes in the circuit.

Over the last several decades, Aharonov-Bohm interferometers have become a paradigm of phase coherent transport and quantum interference in solid state nanostructures[2,3]. In this paper, we analyze an electron Aharonov-Bohm (AB) interferometer consisting of two quantum dots (QDs) connected in parallel to two macroscopic leads such as have been demonstrated experimentally[4–8]. The role of quantum interference and Coulomb interactions in the conductance have been studied using both quantum rate equations (also known as master equations)[9–12] and Greens function technique[13–16]. Earlier theoretical work has also studied the zero frequency shot noise in these structures[17–21].

What distinguishes our work from prior work is the study of spin dependent transport with the inclusion of an inter-dot spin exchange interaction and also the evaluation of the finite frequency shot noise. We show here that the the inclusion of spin-spin interactions, while having no effect on the current-voltage (I-V) curve or zero frequency shot noise, do lead to significant correlations in the finite frequency noise revealing the internal spin dynamics of the interferometer. Both super- and sub-Poissonian correlations, which occur at frequencies corresponding to the intra-dot spin flip Rabi frequencies and inter-dot spin-spin coupling energies, can be further controlled by tuning the magnetic flux through the interferometer. These shot noise correlations occur when each dot is simultaneously occupied by a single electron, which leads to a vanishing of interference fringes in the conductance since intra-dot Coulomb blockade prevents a partitioning of a single electron's wave function between dots. However, the modulation of the shot noise by the AB magnetic flux even in this doubly occupied regime indicates that the relative phase between the electrons still effects the correlation between their tunneling times out of the interferometer. Our approach is based on a master equation for the transport through the dots combined with the quantum regression theorem[23] to calculate the shot noise in the manner originally developed in Refs.[24,25].

The rest of the paper is organized in the following way: in section II we review the model of our system and describe the method used to derive the results; in section III we present and discuss the results, this section is divided into two parts - one considers only results involving zero-flux AB flux and the other the effects of a finite AB flux; section IV summarizes our conclusions.

## II. MODEL

Our model represents a ballistic electron Aharonov-Bohm (AB) interferometer with a single quantum dot embedded in each of the two arms of the interferometer. As shown in Figure 1 both arms are connected in parallel to leads via tunnel barriers. An adjustable bias is applied across the leads allowing the flow of current between them by sequential tunneling of electrons through the dots. Due to the infinite intra-dot Coulomb blockade that we consider, only a single electron can occupy a dot while inter-dot Coulomb charging is finite allowing for double occupancy of the interferometer. An external magnetic field is applied perpendicular to the interferometer leading to a magnetic flux $\Phi$ and Zeeman splitting within the dots. A transverse oscillating radio frequency magnetic field in the plane of the interferometer allows for intra-dot Rabi oscillations between two spin levels with Rabi frequencies $R_1$ and $R_2$ for dot 1 and dot 2, respectively. Finally, we assume the presence of a direct exchange interaction between dots leading to a Heisenberg Hamiltonian for the spins of the two dots in the case of double occupancy characterized by two parameters - the longitudinal coupling ($J_z$) causing a nonlinear Zeeman shift and a transversal coupling strength ($J_n$), which flips the spins. The exchange interaction could arise naturally from tunneling of electrons between dots[26] but also could be induced by, for example, coupling to a superconducting microstrip resonator[27] or by two-photon Raman transitions in an optical microcavity[28,29].
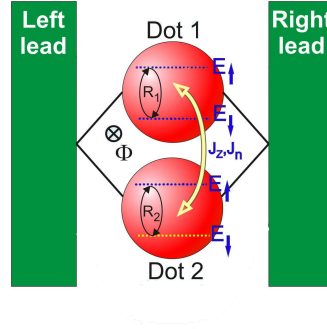


FIG. 1: (Color Online) Model of our system showing two parallel quantum dots coupled to leads with spin exchange interaction between dots. A magnetic field in the region between dots provides a relative phase between electrons in the different dots as a result of the Aharonov-Bohm effect.

The Hamiltonian for the two dot system is given by[29]:

$$
\begin{aligned}
\hat{H} =\ & U\hat{n}_1\hat{n}_2 + \sum_{i=1,2}\left(E_{D,i}\hat{n}_i + \hbar\Omega_i\hat{s}_{i,z}\right) + \\
& + \frac{J_n}{2\hbar}\left(\hat{s}_1^+\hat{s}_2^- + \hat{s}_1^-\hat{s}_2^+\right) + \frac{J_z}{\hbar}\hat{s}_{1,z}\hat{s}_{2,z} \\
& + R_1\left(e^{-i\omega_B t}\hat{s}_1^+ + e^{i\omega_B t}\hat{s}_1^-\right) \\
& + R_2\left(e^{-i\omega_B t}\hat{s}_2^+ + e^{i\omega_B t}\hat{s}_2^-\right) \qquad (1)
\end{aligned}
$$

where $U$ is the inter-dot Coulomb repulsion, $\Omega_i$ is the Zeeman splitting while $E_{D,i}$ is the orbital energy level in dot $i$. $R_1 = -g_1\mu_B B_n/\hbar$ and $R_2 = -g_2\mu_B B_n/\hbar$ are the Rabi frequencies for dot 1 and dot 2, respectively, of the transverse magnetic field oscillating at the frequency $\omega_B$. The operator $\hat{n}_i$ represents the occupation number of dot $i$ while $\hat{s}_{i,z} = \hat{c}_{i,\uparrow}^\dagger\hat{c}_{i,\uparrow} - \hat{c}_{i,\downarrow}^\dagger\hat{c}_{i,\downarrow}$, $\hat{s}_i^- = \hat{c}_{i,\downarrow}^\dagger\hat{c}_{i,\uparrow}$, $\hat{s}_i^+ = \hat{c}_{i,\uparrow}^\dagger\hat{c}_{i,\downarrow}$ are the spin operators for an electron in dot $i$ and $\hat{c}_{i,\sigma}$ is a spin-$\sigma$ electron annihilation operator for dot $i$.

After transforming the spin operators to a frame rotating at the transverse field frequency $\omega_B$, the Hamiltonian becomes,

$$
\begin{aligned}
\hat{H} =\ & U\hat{n}_1\hat{n}_2 + \sum_{i=1,2}\left(\bar{E}_D\hat{n}_i + \Delta\hat{s}_{i,z}\right) + \\
& + \frac{J_n}{2\hbar}\left(\hat{s}_1^+\hat{s}_2^- + \hat{s}_1^-\hat{s}_2^+\right) + \frac{J_z}{\hbar}\hat{s}_{1,z}\hat{s}_{2,z} \\
& + R_1\left(\hat{s}_1^+ + \hat{s}_1^-\right) + R_2\left(\hat{s}_2^+ + \hat{s}_2^-\right) \qquad (2)
\end{aligned}
$$

where $\Delta = \bar{\Omega} - \omega_B$ is the detuning of the RF magnetic field relative to the average Zeeman splitting. We have assumed that the difference in the orbital energy levels and Zeeman splitting of the dots are small compared to all other characteristic energies, $|E_{D,1} - E_{D,2}|, |\Omega_1 - \Omega_2| \ll \bar{E}_D, \bar{\Omega}, R_1, R_2, J_n, J_z$ so that from henceforth we can assume that the differences can be neglected and the average orbital and Zeeman energies, $\bar{E}_D$ and $\bar{\Omega}$, can be used instead. This approximation is important for the operation of the device as an interferometer since for large $|E_{D,1} - E_{D,2}|, |\Omega_1 - \Omega_2|$ the symmetry between paths of the interferometer with respect to the leads is ruined and there is no longer any observable interference.

The energy diagram of our system is presented in Figure 2(b) along with the transition energies $\Delta E$ in (a) representing the energy required to add an additional electron to the device from the leads. These are the energies that an electron in a lead needs to have in order to tunnel into one of the two spin-states of an empty dot. In the case of one empty and one occupied dot, the inter-dot Coulomb repulsion $U$ between electrons increases the needed energy of an electron to enter the empty dot by U to $E_D \pm \Omega + U$. Naturally, this increases the energy levels of our system (shown in Figure2(b)) for the doubly occupied states.
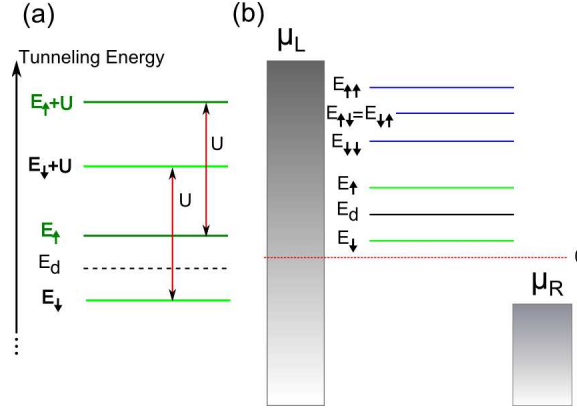


FIG. 2: (Color Online) Depiction of energy parameters of interest in our model (not to scale): (a) diagram of tunneling energies, (b) energy eigenstates of the double dot for $R_1 = R_2 = J_n = J_z = 0$. $E_\sigma$ represents a single spin polarized electron in the interferometer with spin $\sigma$ while $E_{\sigma\sigma'}$ represent one electron in each of the dots with spins $\sigma$ and $\sigma'$.

The coupling between the leads and the dots is described by the Hamiltonian[9–16,18–21]:

$$\hat{H}_{lead-dot} = \sum_{k,\sigma} \left( t_{L1\sigma} \hat{d}_{Lk\sigma}^\dagger \hat{c}_{1,\sigma} + t_{R1\sigma} \hat{d}_{Rk\sigma}^\dagger \hat{c}_{1,\sigma} + h.c. \right)$$
$$+ \sum_{k,\sigma} \left( t_{L2\sigma} \hat{d}_{Lk\sigma}^\dagger \hat{c}_{2,\sigma} + t_{R2\sigma} \hat{d}_{Rk\sigma}^\dagger \hat{c}_{2,\sigma} + h.c. \right) \quad (3)$$

where $\hat{d}_{L(R)k\sigma}$ is the annihilation operator for an electron in the left(right) lead with momentum $k$ and spin $\sigma$ and $t_{L(R)i\sigma}$ is the tunneling amplitude of that electron across the tunnel barrier into the $i^{th}$ dot. The AB phase $\Phi$ due to the magnetic flux is be incorporated into the tunneling amplitudes[9–16], $t_{L1\sigma}^* = t_{L2\sigma} = t_{R2\sigma}^* = t_{R1\sigma} = |t|e^{i\Phi/4}$, where we assume for simplicity that the tunneling amplitudes are the same for both leads.

In order to incorporate the coupling of the dots to the left and right macroscopic leads, we introduce the density matrix whose elements are defined as

$$\rho_{\sigma_1',\sigma_2',\sigma_1,\sigma_2} = \langle \sigma_1', \sigma_2' | \hat{\rho} | \sigma_1, \sigma_2, \rangle$$

where $|\sigma_1, \sigma_2'\rangle$ represents a state with electron with spin $\sigma_1 = 0, \uparrow, \downarrow$ in the first dot and an electron with spin $\sigma_2' = 0, \uparrow, \downarrow$ in the second dot (0 indicates an empty dot). The time evolution of $\rho$ is given by a Born-Markov master equations consisting of two parts:

$$\dot{\rho} = -(i/\hbar)[\hat{H}, \rho] + \mathbf{L}[\rho] \quad (4)$$

Here the first term of the master equation represents the unitary evolution due to the Hamiltonian. The second part represents the coupling to the leads, which can be derived from $\hat{H}_{lead-dot}$ using either Greens functions[9,22] or second order perturbation theory on the density operator[25],

$$\dot{\rho}_{00,00} = \sum_\sigma [-2\alpha_{1\sigma}\rho_{00,00} + \beta_{1\sigma}(\rho_{\sigma0,\sigma0} + \rho_{0\sigma,0\sigma}) +$$

$$+ \quad \beta_{2\sigma}\rho_{\sigma0,0\sigma} + \beta_{2\sigma}^*\rho_{0\sigma,\sigma0}]$$

$$\dot{\rho}_{\sigma0,\sigma0} = \alpha_{1\sigma}\rho_{00,00} - (\beta_{1\sigma} + \sum_{\sigma'}\tilde{\alpha}_{1\sigma'})\rho_{\sigma0,\sigma0}$$
$$- \quad 1/2(\beta_{2\sigma} + \tilde{\alpha}_{2\sigma})\rho_{\sigma0,0\sigma} - 1/2(\beta_{2\sigma}^* + \tilde{\alpha}_{2\sigma}^*)\rho_{0\sigma,\sigma0}$$
$$+ \quad \sum_{\sigma'}\tilde{\beta}_{1\sigma'}\rho_{\sigma\sigma',\sigma\sigma'}$$

$$\dot{\rho}_{0\sigma,0\sigma} = \alpha_{1\sigma}\rho_{00,00} - (\beta_{1\sigma} + \sum_{\sigma'}\tilde{\alpha}_{1\sigma'})\rho_{0\sigma,0\sigma}$$
$$- \quad 1/2(\beta_{2\sigma} + \tilde{\alpha}_{2\sigma})\rho_{\sigma0,0\sigma} - 1/2(\beta_{2\sigma}^* + \tilde{\alpha}_{2\sigma}^*)\rho_{0\sigma,\sigma0}$$
$$+ \quad \sum_{\sigma'}\tilde{\beta}_{1\sigma'}\rho_{\sigma'\sigma,\sigma'\sigma}$$

$$\dot{\rho}_{0\sigma,\sigma0} = \alpha_{2\sigma}\rho_{00,00} - 1/2(\beta_{2\sigma} + \tilde{\alpha}_{2\sigma})(\rho_{\sigma0,\sigma0} + \rho_{0\sigma,0\sigma})$$
$$- \quad (\beta_{1\sigma} + \sum_{\sigma'}\tilde{\alpha}_{1\sigma'})\rho_{0\sigma,\sigma0} + \tilde{\beta}_{2\sigma}\rho_{\sigma\sigma,\sigma\sigma}$$

$$\dot{\rho}_{\sigma\sigma,\sigma\sigma} = \tilde{\alpha}_{1\sigma}(\rho_{\sigma0,\sigma0} + \rho_{0\sigma,0\sigma}) + \tilde{\alpha}_{2\sigma}\rho_{\sigma0,0\sigma}$$
$$+ \quad \tilde{\alpha}_{2\sigma}^*\rho_{0\sigma,\sigma0} - 2\tilde{\beta}_{1\sigma}\rho_{\sigma\sigma,\sigma\sigma},$$

$$\dot{\rho}_{\sigma\bar{\sigma},\sigma\bar{\sigma}} = \tilde{\alpha}_{1\sigma}\rho_{0\bar{\sigma},0\bar{\sigma}}$$
$$+ \quad \tilde{\alpha}_{1\bar{\sigma}}\rho_{\sigma0,\sigma0} - (\tilde{\beta}_{1\sigma} + \tilde{\beta}_{1\bar{\sigma}})\rho_{\sigma\bar{\sigma},\sigma\bar{\sigma}} \quad (5)$$

where tunneling rates $\alpha_{1\sigma}(\tilde{\alpha}_{1\sigma})$ model the tunneling out of the leads into singly (doubly) occupied dot states while $\alpha_{2\sigma}(\tilde{\alpha}_{2\sigma})$ by contrast model the tunneling out of the leads into a superposition of singly (doubly) occupied states, respectively, where the wave function of the entering electron is split between the dots. Coefficients $\beta_{1\sigma}(\tilde{\beta}_{1\sigma})$ and $\beta_{2\sigma}(\tilde{\beta}_{2\sigma})$ are the tunneling rates out of singly (doubly) occupied dots and the appropriate superpositions into the leads. These tunneling rates are given explicitly in terms of the Fermi-Dirac distribution of the leads $f_{L(R)}(\epsilon)$, the probability per unit time of an electron crossing the tunnel barrier from the lead into one of the dots or vice versa $\Gamma_{L(R)\sigma} \propto |t|^2$, and the AB magnetic flux enclosed by the interferometer $\Phi$:

$$\alpha_{1\sigma} = f_L(E_\sigma)\Gamma_{L\sigma} + f_R(E_\sigma)\Gamma_{R\sigma}$$
$$\beta_{1\sigma} = (1 - f_L(E_\sigma))\Gamma_{L\sigma} + (1 - f_R(E_\sigma))\Gamma_{R\sigma}$$
$$\tilde{\alpha}_{1\sigma} = f_L(E_\sigma + U)\Gamma_{L\sigma} + f_R(E_\sigma + U)\Gamma_{R\sigma}$$
$$\tilde{\beta}_{1\sigma} = (1 - f_L(E_\sigma + U))\Gamma_{L\sigma} + (1 - f_R(E_\sigma))\Gamma_{R\sigma}$$
$$\alpha_{2\sigma} = f_L(E_\sigma)\Gamma_{L\sigma}e^{-i\Phi/2} + f_R(E_\sigma)\Gamma_{R\sigma}e^{i\Phi/2}$$
$$\beta_{2\sigma} = (1 - f_L(E_\sigma))\Gamma_{L\sigma}e^{-i\Phi/2} + (1 - f_R(E_\sigma))\Gamma_{R\sigma}e^{i\Phi/2}$$
$$\tilde{\alpha}_{2\sigma} = f_L(E_\sigma + U)\Gamma_{L\sigma}e^{-i\Phi/2} + f_R(E_\sigma + U)\Gamma_{R\sigma}e^{i\Phi/2}$$
$$\tilde{\beta}_{2\sigma} = (1 - f_L(E_\sigma + U))\Gamma_{L\sigma}e^{-i\Phi/2}$$
$$+ \quad (1 - f_R(E_\sigma + U))\Gamma_{R\sigma}e^{i\Phi/2} \quad (6)$$

The equations for the tunneling coefficients clearly demonstrate the influence of the magnetic flux $\Phi$ in the terms $\alpha_{2,\sigma}$, $\tilde{\alpha}_{2,\sigma}$, $\beta_{2,\sigma}$, and $\tilde{\beta}_{2,\sigma}$ as the relative phase factor $\exp(-i\Phi)$ between the probability amplitude for tunneling into the left and right leads.

To numerically calculate the shot noise we first rewrite the quantum rate equations in matrix form:

$$\frac{d\vec{\rho}(t)}{dt} = \mathbf{M}\vec{\rho}(t) \quad (7)$$

where $\vec{\rho}(t)$ is the column vector of the density matrix elements, $\rho_{\sigma\sigma',\sigma''\sigma'''} = \langle\sigma,\sigma'|\hat{\rho}|\sigma'',\sigma'''\rangle$ given in appendix A. The noise power spectrum for the current is given by Fourier transform of the current-current correlation function:

$$S_{I_{j,a}I_{j',a}}(\omega) = 2\int_{-\infty}^{\infty}dt e^{i\omega t}\left[\langle I_{j,a}(t)I_{j',a}(0)\rangle - \langle I_{j,a}\rangle\langle I_{j',a}\rangle\right](8)$$

where $I_{j,a}$ is either spin or charge current ($a = C, S$) through the lead $j = L, R$. Spin current is defined as

$$I_{j,S} = \frac{\hbar}{2}(I_{j,\uparrow} - I_{j,\downarrow}) = \frac{\hbar}{2}Tr[(\hat{\Gamma}_{j,\uparrow} - \hat{\Gamma}_{j,\downarrow})\vec{\rho}^{(0)}], \quad (9)$$

while charge current is given by

$$I_{j,C} = e\left(I_{j,\uparrow} + I_{j,\downarrow}\right) = eTr[\left(\hat{\Gamma}_{j,\uparrow} + \hat{\Gamma}_{j,\downarrow}\right)\vec{\rho}^{(0)}] \tag{10}$$

where $\vec{\rho}^{(0)}$ is the steady-state solution of equation (7) given by the eigenvector of the zero eigenvalue of $\mathbf{M}$. The current operator $\hat{\Gamma}_{j,\sigma}$ contains the rates for spin $\sigma$ electron tunneling across $j = L, R$ lead into or out of the appropriate states of the dots. These operators are completely defined by the rate of change of the populations due to tunneling with detailed expressions given in appendix A.

By introduction of the time evolution operator $\hat{T}(t) = exp\left[\mathbf{M}t\right]$ and subsequent spectral decomposition of matrix $\mathbf{M}$, one obtains the expression for the shot noise spectrum[24],

$$
\begin{aligned}
S_{I_{j,\sigma}I_{j',\sigma'}}(\omega) \ = \ & \delta_{j,j'}\delta_{\sigma,\sigma'}2sI_{j,\sigma} \\
& + \ 2s^2 \sum_{\lambda \neq 0} \left( \frac{Tr\left[\hat{\Gamma}_{j,\sigma}\hat{P}_\lambda\hat{\Gamma}_{j',\sigma'}\vec{\rho}^{(0)}\right]}{-i\omega - \lambda} + \right. \\
& + \ \left. \frac{Tr\left[\hat{\Gamma}_{j',\sigma'}\hat{P}_\lambda\hat{\Gamma}_{j,\sigma}\vec{\rho}^{(0)}\right]}{i\omega - \lambda} \right)
\end{aligned}
\tag{11}
$$

where $s = e$ for charge current and $s = \frac{\hbar}{2}$ for spin current. Here the $\lambda$'s are the eigenvalues of the matrix $\mathbf{M}$ while $\hat{P}_\lambda$ is the projection matrix that projects a vector onto the subspace spanned by the eigenvalue $\lambda$.

The Fano factor, which measures the ratio of the actual shot noise to Poissonian Schottky noise of uncorrelated particles, $2sI$, is given by:

$$F_{C(S)}(\omega) = \frac{S_{C(S)}(\omega)}{2sI_{C(S)}} \tag{12}$$

where $S_{C(S)}(\omega)$ is the charge (C) or spin (S) shot noise in the right lead. Because the number of electrons passing from the left to the right lead is conserved, both the average current and the shot noise are identical in both leads.

## III. RESULTS

In the first subsection we examine the current vs. lead voltage and shot noise for the particular case of zero magnetic flux in detail and then we examine how the nonzero AB flux modifies these results in the subsequent subsection. In all our calculations, we set the tunneling rates between the leads and the dots to be equal, $\Gamma_{L(R)\sigma} = \Gamma$ and use $\Gamma$ as the energy/time scale relative to which all energies and frequencies are measured. We therefore calculate the charge current $I_C$ in units of $e\Gamma$ and the spin current $I_S$ in units of $\hbar\Gamma/2$. We consider the dots to be identical with the single-electron level $E_d = 5$, Zeeman splitting $\Omega = 4$, and inter-dot Coulomb repulsion $U = 20$ (in units of $\hbar\Gamma$). The voltage bias $\Delta V = \mu_L - \mu_R$ across the leads is symmetric about zero with $\mu_L = -\mu_R$ and is expressed everywhere in units of $\hbar\Gamma/|e|$. Additionally, we consider both unpolarized leads containing both spin polarizations as well ferromagnetic leads with identical polarization or opposite polarizations. Although we have examined both charge and spin shot noise, in the rest of the paper we have presented only charge shot noise graphs, because the spin shot noise shows the same features as charge noise and does not provide any additional information.

### A. Zero flux

In Figure 3 we show the behavior of spin and charge currents through the device versus $\Delta V$ in the absence of the external magnetic flux ($\Phi = 0$) as well as Rabi oscillations ($R_1 = R_2 = 0$) and exchange coupling ($J_n = J_z = 0$) for unpolarized leads. The charge I-V curve exhibits an expected "staircase" behavior, ascending in steps and reaching higher and higher plateaus as the potential of the left lead $\mu_L$ crosses higher energy levels and opens additional transport channels. Unlike charge current, the spin current displays a qualitatively different I-V curve. For low bias, $\Delta V < 2$, electrons in the leads do not have enough energy to tunnel into the dots and both spin and charge currents are zero. As the potential of the left lead increases over the single spin-down tunneling energy $E_{TUN\downarrow} = E_D - \Omega$, only a spin down electron can enter the dots and the spin current becomes negative, while charge current is positive. When the left lead potential crosses the value of the spin-up electron tunneling energy $E_{TUN\uparrow} = E_D + \Omega$, both spin

up and down currents are equal leading to zero total spin current but another jump in the charge current. Once $\mu_L$ crosses the tunneling energy needed for an additional spin-down electron to tunnel into the single empty dot, $E'_{TUN\downarrow} = E_\downarrow + U$, three new transport channels open up - $E_{\downarrow\downarrow}, E_{\uparrow\downarrow}$ and $E_{\downarrow\uparrow}$ - leading to another jump in the charge current. Since only doubly occupied states with at least one spin down electron are now accessible from the left lead an "imbalance" between spin-up and spin-down current is established once again and there is a non-zero total spin current. Finally after a further increase in $\mu_L$ of $2\bar{\Omega}$, a second spin up electron is now able to enter thereby again restoring the symmetry between spin up and down electrons. This results in the spin current again returning to zero but a final jump in the charge current. Figure 4 shows the charge and spin current shot noise in each of the plateau regions showing sub-Poissonian statistics at zero frequency and Poissonian statistics at finite frequencies.
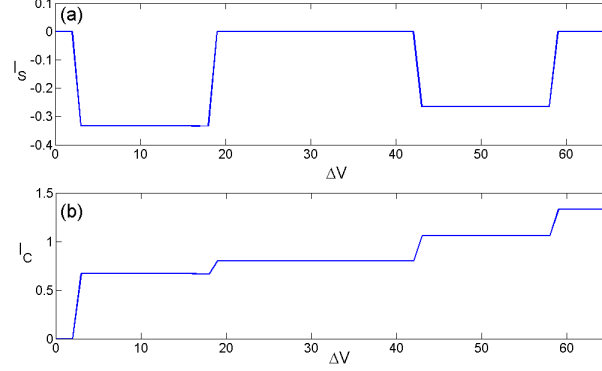


FIG. 3: (Color Online) I-V curve in the absence of magnetic flux for $U = 20, R_1 = R_2 = 0$ and $J_z = J_n = 0$ (unpolarized leads): (a) spin current, (b) charge current. Note that here and in all subsequent graphs $I_C$ is in units of $e\Gamma$ and $I_S$ is in units of $\hbar\Gamma/2$ while $\Delta V$ is in units of $\hbar\Gamma/|e|$.
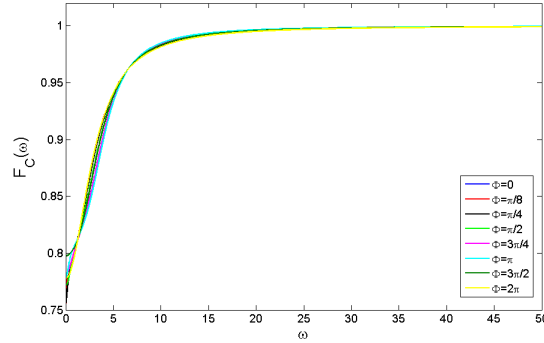


FIG. 4: (Color Online) Charge current shot noise as a function of frequency for $U = 20, R_1 = R_2 = 0, J_z = J_n = 0$ and different values of magnetic flux (unpolarized leads). Note that here and in all subsequent figures $\omega$ is measured in units of $\Gamma$.

It is clear from Eq. 1 that the exchange coupling functions only when both dots are occupied by an electron. Therefore to study it's effect we let $\Delta V \to \infty$ so that all single and doubly occupied states are accessible transport channels regardless of the Rabi frequencies and exchange coupling energies. In this case there are no visible effects of the exchange coupling on the total spin and charge currents since no new transport channels are created by either the Rabi spin flips or the exchange coupling. These interactions couple the bare energy eigenstates of the dots leading to a new basis of energy eigenstates of the same dimension. The same is true of the zero frequency shot noise. From Figure 4 one can see that $F(0) \approx 0.77$. The same value of $F(0)$ is obtained for the parameters plotted in 5, 6, 7 and 8 showing that $F(0)$ is independent of $\Phi$, $R_{1,2}$, $J_n$, and $J_z$. $F(0)$ is a direct measure of the number of open transport channels $N$,

$$F(0) = \frac{\sum_{n=1}^{N} T_n(1 - T_n)}{\sum_{n=1}^{N} T_n} \tag{13}$$

where $T_n$ is the transmission probability through one of the open channels and is not expected to depend on the interactions in the large bias limit.

However, the effect of both intradot spin flips and exchange coupling between dots do manifest themselves in the frequency dependent shot noise as can be seen in Figures 5, 6, 7 and 8. In the absence of Rabi oscillations the shot noise is sub-Poissonian in the low-frequency range, and quickly becomes Poissonian for higher frequencies. In the case of non-zero spin Rabi flopping and $\Delta V \to \infty$ the shot noise spectrum exhibits structures characteristic of Fano resonances visible at frequencies equal to twice the Rabi frequencies, $\omega = 2R_i, i = 1, 2$ when the leads are spin polarized (in the case of unpolarized leads, there is no observable effect even for the spin current). Similar finite frequency shot noise resonances have been studied for spin Rabi flopping in a single quantum dot[30] and for double quantum dots in series with inter-dot tunneling[24] and can be explained as follows: For leads with identical spin polarization, an electron can only exit through the right lead allowing another electron to enter the same dot if it either undergoes no Rabi flopping or a full $2\pi$ Rabi oscillation. The case of no Rabi oscillation contributes only to the zero frequency noise. For leads of opposite polarization, two successive electrons must undergo $1/2$ of a Rabi oscillation to exit leading to current correlations at intervals $\pi/2R_i + \pi/2R_i = \pi/R_i$. The current therefore exhibits positive super-Poissonian correlations at time intervals $\pi/R_i$ corresponding to a frequency $\omega = 2R_i$.

In the same figures one can also see how the exchange coupling affects these resonances. As can be seen in Figure 5, an increase in the longitudinal coupling $J_z$ affects the position of the structures in the shot noise moving them away from each other by shifting the low frequency structure towards even lower frequencies and the high frequency one towards even higher frequencies. This can be qualitatively understood by noting that the longitudinal coupling shifts the Zeeman splitting of each spin by an amount $\pm J_z$ depending on the orientation of the spin in the adjacent dot leading to off-resonant Rabi oscillations at the frequencies $\sqrt{R_i^2 + (\Delta \pm J_z)^2}$. Changing the value of the transverse exchange coupling $J_n$ not only effects the position but also the number of non-Poissonian resonances in the shot noise as shown in Figure 6. When $R_1 \neq R_2$ there are two Fano-shaped structures in the shot noise spectrum (see Fig6(a)) but once $J_n$ becomes non-zero each of the structures bifurcates into two resonances located symmetrically around $\omega = 2R_i$ separated by $2J_n$. Since the transverse exchange $J_n$ represents non-linear Rabi oscillations where the spin state of the first dot undergoes oscillations conditioned on the presence of another electron in the second dot, which also Rabi flops in response to the first electron, $J_n$ acts in conjunction with the single spin linear Rabi flopping to give rise to Rabi oscillations at the frequencies $R_i \pm J_n$ where the $\pm$ results from the relative orientations of the spins.
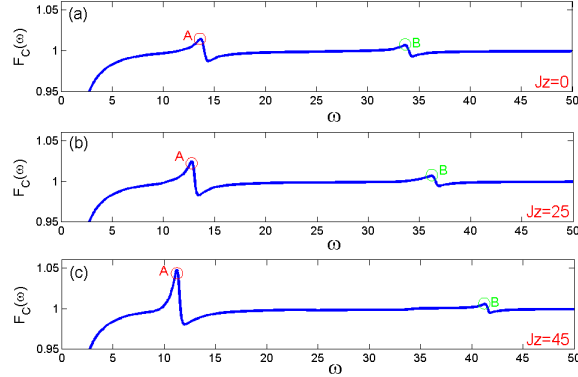


FIG. 5: (Color Online) The effect of the longitudinal direct spin coupling strength $J_z$ on a charge current shot noise as a function of frequency (identical lead polarizations), (a) $J_z = 0$, (b) $J_z = 25$, and (c) $J_z = 45$. For all graphs $\Delta V = 80, \Phi = 0, U = 20, R_1 = 7, R_2 = 17$, and $J_n = 0$.

Lastly, it is worth remarking on the effect the polarization of the leads has on the shape of the resonances. In Figure 7(a) we have plotted the shot noise for a range of $J_z$ in the case of identical polarization, and in Figure 8(a) for the case of opposite polarization. Figures 7(b) and 8(b) also show the shot noise for the same polarizations but for a range of $J_n$. In both cases one can see that the shape of the resonances are inverted when leads are changed from identical polarization to opposite polarization, i.e. for identical polarization the peak-feature of the structure is followed by the dip feature while in the case of opposite polarization the dip precedes the peak. This is not unique to the case of zero magnetic flux either as one can see from Figs. 12(a) and 12(b) in the next section where the shape of the resonances are inverted when the lead polarizations are changed irrespective of the flux through the interferometer. For identical lead polarizations the dominant super-Poissonian peaks representing bunching of electrons change to a sub-Poissonian anti-bunching when the polarization of the right lead is inverted. For identical polarizations it is easy for successive electrons to transit through the dot since a spin flip is not necessary leading to bunching whereas for opposite polarizations a spin flip becomes necessary for each of the electrons leading to an increase in the time

between electron arrivals and hence antibunching of the arrival times in the lead.
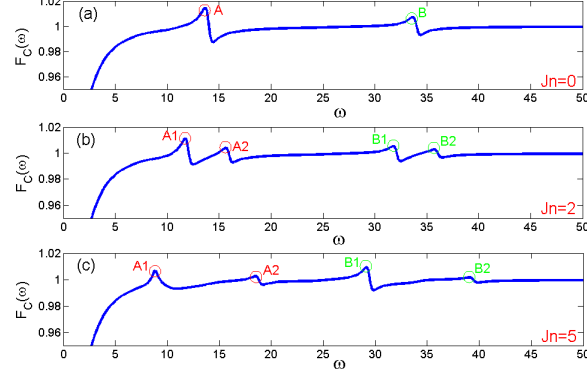


FIG. 6: (Color Online) The effect of the transversal direct spin coupling strength $J_n$ on a charge current shot noise as a function of frequency (identical lead polarizations), (a) $J_n = 0$, (b) $J_n = 2$, and (c) $J_n = 5$. For all graphs $\Delta V = 80, \Phi = 0, U = 20, R_1 = 7, R_2 = 17$, and $J_z = 0$.
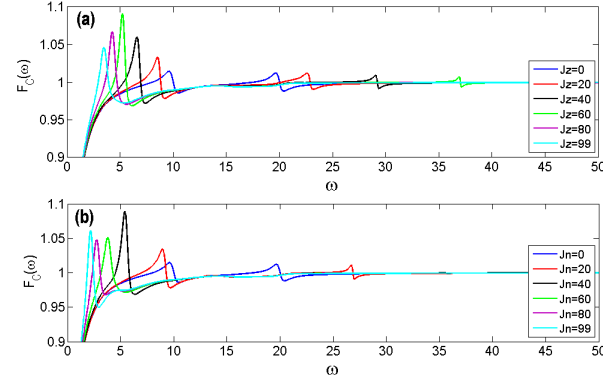


FIG. 7: (Color Online) Charge current shot noise as a function of frequency for $\Delta V = 80$, inter dot Coulomb blockade $U = 20$, AB phase $\Phi = 0$ and Rabi frequencies $R_1 = 10, R_2 = 5$ (identical lead polarizations): (a) for the range of values of parameter $J_z$, (b) for the range of values of parameter $J_n$.

## B. Finite flux

The spin and charge I-V curves for different values of $\Phi$ are shown in figures 9 and 10. Here we draw attention to two distinct cases - one when there is a difference between the Rabi frequencies (Fig. 9) and the other when the Rabi frequencies are identical (Fig. 10). In the former case, shown in figure 9, the I-V curve is completely independent of $\Phi$ indicative of no interference between paths in the conductance. The absence of flux-dependent interference is because the difference in the Rabi frequencies introduces clear "which-way" information for the path an electron takes in the form of the spin orientation of the electron exiting the interferometer. For identical Rabi frequencies (Fig10) there is no distinction between the two dots and "which-way" information is not present. In this case one can see the strong dependence of the charge current on the AB flux. The spin current only exhibits interference in the bias ranges where there is an unbalanced number of transport channels for spin down electrons.

Figure 11(a-c) shows $I_C$ as a function of $(\Phi)$ for three different $\Delta V$ for $J_n = J_z = 0$ and $R_1 = R_2 = 0$. In Fig.11(a) where $E_d - \Omega < \Delta V < E_d + U - \Omega$ there is only single electron occupancy of the interferometer resulting in a high contrast interference pattern with constructive interference at integer multiples of $2\pi$ and total destructive interference at odd multiples of $\pi$. In the transitional regime, $E_d + U - \Omega < \Delta V < E_d + U + \Omega$, where all doubly occupied states are allowed, an AB interference pattern is still visible but now total destructive interference occurs only at integer multiples of $4\pi$. For large bias values, $\Delta V > E_d + U + \Omega$, all doubly occupied states are equally probable and there are no AB oscillations since the Coulomb blockade causes the two electrons to be partitioned equally between the
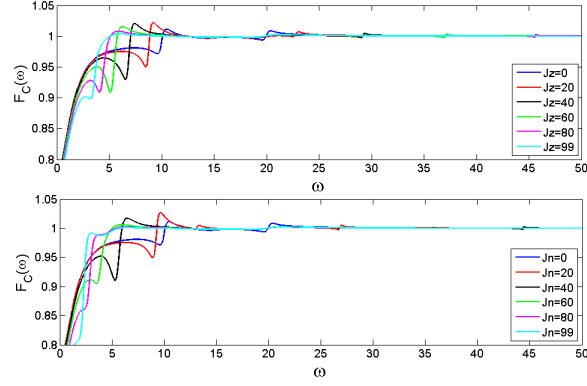
FIG. 8: (Color Online) Charge current shot noise as a function of frequency for $\Delta V = 80$, inter-dot Coulomb blockade $U = 20$, AB phase $\Phi = 0$ and Rabi frequencies $R_1 = 10, R_2 = 5$ (opposite lead polarizations): (a) for the range of values of parameter $J_z$, (b) for the range of values of parameter $J_n$.
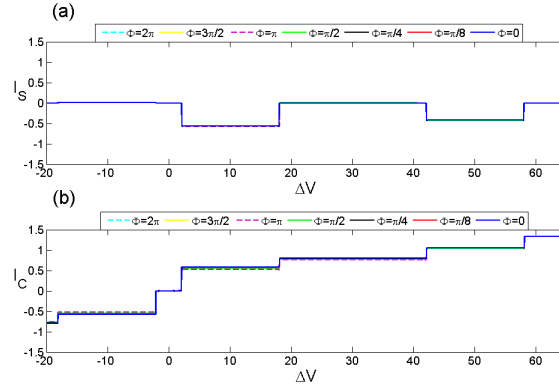


FIG. 9: (Color Online) I-V curve for $U = 20, R_1 = 10, R_2 = 5, J_n = J_z = 0$ and different values of AB flux (unpolarized leads): (a) spin current, (b) charge current.

dots with zero probability of two electrons on the same dot. In this context the partial interference seen in Fig.11(b) can be attributed to the absence of $| \uparrow_1, \uparrow_2 \rangle$. Equal non-zero Rabi oscillations do not change $I_C$ vs. $\Phi$ while an increase in the difference between the two Rabi frequencies makes the AB oscillation more harmonic while reducing the amplitude of the oscillations since again the difference between $R_1$ and $R_2$ provides "which way" information for the interferometer. This is shown in Fig. 11(d).

The effect of $\Phi$ on the shot noise in the limit of very large bias ($\Delta V \rightarrow \infty$) is shown in Figure 12. While $F(0)$ is unaffected by the AB flux, there is a reduction in the size of the Fano-style resonances at finite frequency. In the case of identical lead polarizations (Fig12(a)), as the flux increases to $\Phi = \pi$ there is a dramatic attenuation of the amplitude of the high frequency resonance eventually causing the shape of the resonance to invert itself at $\Phi = \pi$. The low frequency resonance shows significantly less attenuation with increasing $\Phi$. After $\Phi$ crosses the value of $\pi$ the attenuation reverses and the features grow in amplitude again for increasing $\Phi$, returning to their maximum amplitude at $\Phi = 2\pi$. For opposite lead polarizations we have a similar attenuation of the noise resonances, only in this case it is more visible in the lower-frequency structure.

## IV. CONCLUSIONS

We have examined a ballistic electron double-dot Aharonov-Bohm interferometer with a focus on the effect that inter-dot spin-spin interactions and intra-dot spin flips have on the current and frequency dependent current shot noise. Direct spin exchange coupling ($J_z$ and $J_n$) have no effect on either the spin or charge currents or zero frequency shot noise but do effect the shot noise at finite frequencies. For nonzero intra-dot spin flips, the shot noise displays characteristic resonances at twice the Rabi frequencies whose's positions are shifted by $J_z$ and are split into pairs of resonances by $J_n$. These results indicate that spin interactions between quantum dots can be measured directly from
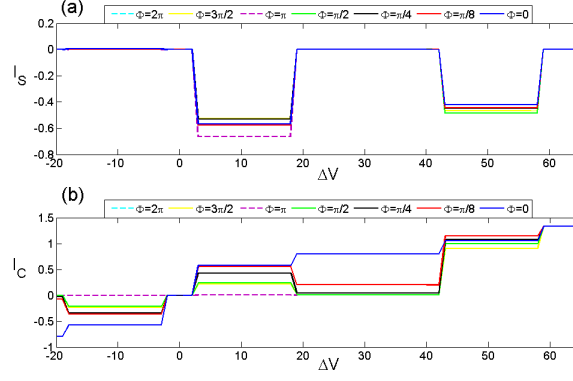
FIG. 10: (Color Online) I-V curve for $U = 20, R_1 = 10, R_2 = 10, J_n = J_z = 0$ and different values of AB flux (unpolarized leads): (a) spin current, (b) charge current.
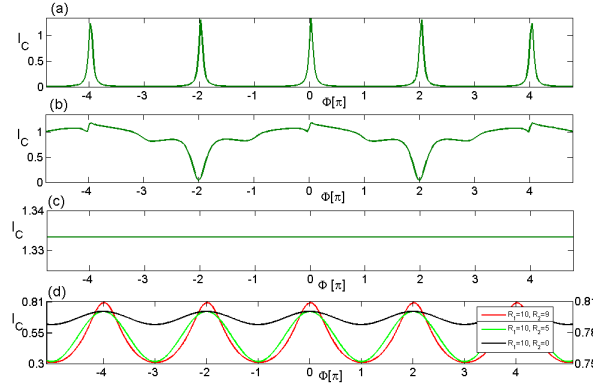


FIG. 11: (Color Online) Charge current as a function of AB flux (in units of $\pi$) for $U = 20, R_1 = R_2 = 0, J_n = 0$, and $J_z = 0$(unpolarized leads): (a) small bias $\Delta V = 20$, (b) medium bias $\Delta V = 46$, (c) large bias $\Delta V = 80$, and (d) small bias $\Delta V = 20$ - different Rabi frequencies ($R_1 = R_2 = 10$ on the left y-axis, $R_1 = 10, R_2 = 5$ and $R_1 = 10, R_2 = 0$ on the right axis).

the finite frequency charge shot noise. The effect of finite AB flux through the interferometer also affects the shot noise resonances leading to an attenuation of their amplitude for phases increasing from 0 to $\pi$ reflecting increased destructive interference while the amplitudes again grow in the interval $\pi$ to $2\pi$ as destructive interference gives way to constructive interference.

Experiments have already been performed on parallel coupled quantum dots that function as an AB interferometer[4,5,7] and on double dots with spin exchange interaction due to tunneling of electrons between the dots[26] both using gate defined quantum dots in two dimensional electron gases (2DEG) formed at AlGaAs/GaAs interfaces. In fact, the AB interferometer experiments[4,5,7] also included a tunable tunnel coupling between dots but the experiments did not study the spin state whereas the latter experiment[26] explicitly used the tunnel coupling to lift the degeneracy between spin singlet and triplet states to coherently control the two electron spin states of the double dot. What would be required for our model is to to repeat the previous experiments[4,5,7] but with spin polarized leads. In the last decade there have been numerous demonstrations of spin injection and spin measurements in semiconductors[31]. Injection of spin polarized charge carriers into nonmagnetic GaAs leads can be achieved either from a ferromagnetic doped semiconductor layer such as GaMnAs[32] or from ferromagnetic metallic layers such as CoFe via a tunnel barrier[33].

In a future work we will quantify the level entanglement between the dots and how the shot noise spectrum correlates with the measures of entanglement. It has been shown[34] that the entanglement of two electrons in the double-dot can be detected in noise measurements, where singlet and triplet states lead to noise contributions of opposite signs. By appropriate control of AB phase, inter-dot Coulomb repulsion, and inter-dot spin-spin coupling one can manipulate the probability amplitudes for the different tunneling paths of the interferometer and the probability of formation of inter-dot entangled spin triplet and singlet states.
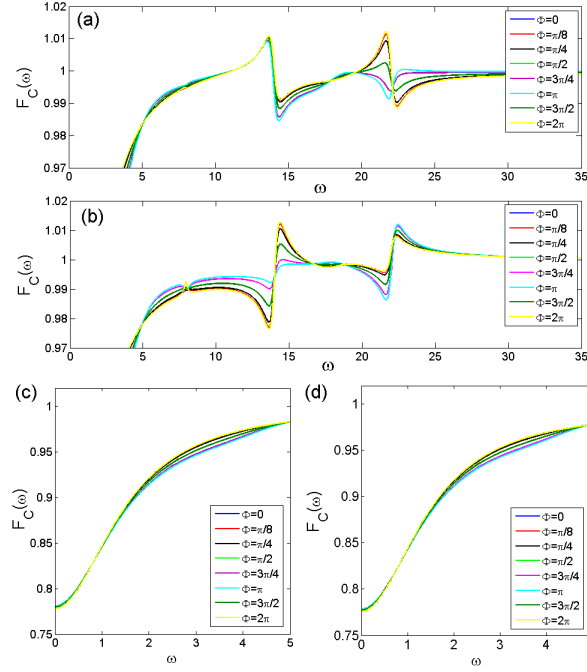
FIG. 12: (Color Online) Charge current shot noise as a function of frequency for $\Delta V = 80, U = 20, R_1 = 7, R_2 = 11, J_n = 0, J_z = 0$ and different values of AB flux: (a) identical lead polarizations and (b) opposite lead polarizations. (c) and (d) are closeups of (a) and (b), respectively, showing the shot noise for low frequencies.

## V.   ACKNOWLEDGEMENTS

## VI.   REFERENCES

[1] C. Beenakker and C. Schonenberger, Physics Today **56**, 37-42 (2003); Ya. M. Blanter and M. Buttiker, Phys. Rep. **336**, 1-166 (2000).

[2] A. Yacoby, M. Heiblum, D. Mahalu, H. Shtrikman, Phys. Rev. Lett. **74**, 47-50 (1994).

[3] Y. Ji, Y. Chung, D. Sprinzak, M. Heiblum, D. Mahalu, and H. Shtrikman, Nature **422**, 415-418 (2003).

[4] Alexander W. Holleitner, Robert H. Blick, Andreas K. Huttel, Karl Eber, Jorg P. Kotthaus, Science **297** 70 (2002).

[5] A.W. Holleitner, C.R. Decker, H. Qin, K. Eber, and R. H. Blick, Phys. Rev. Lett. **87**, 256802 (2001).

[6] J. C. Chen, A.M. Chang, and M. R. Melloch, Phys. Rev. Lett. **92** 176801 (2004).

[7] R.H. Blick, A.K. Huttel, A.W. Holleitner, E.M. Hohberger, H. Qin, J. Kirschbaum, J. Weber, W. Wegscheider, M. Bichler, K. Eberl, J.P. Kotthaus, Physica E, **16**, 76 (2003).

[8] Martin Sigrist, Thomas Ihn, Klaus Ensslin, Matthias Reinwald, and Werner Wegscheider, Phys. Rev. Lett. **98**, 036805 (2007).

[9] J. Ma, B. Dong, and X. L. Lei, The European Physical Journal B **36**, 599-605 (2003).

[10] B. Dong, I. Djuric, H. L. Cui, and X. L. Lei, J. Phys.: Condens. Matter **16**, 4303-4314 (2004).

[11] Bing Dong, X. L. Lei, N. J. M. Horing, Phys. Rev. B **77**, 085309 (2008).

[12] Y Tokura, H Nakano, and T Kubo, New Journal of Physics **9**, 113 (2007).

[13] D. Sztenkiel and R. Swirkowicz, J. Phys. C: Condens. Matter **19** 176202 (2007).

[14] Haizhou Lu, Rong Lu, and Bang-fen Zhu, Phys. Rev. B **71**, 235320 (2005).

[15] Jin-Liang Li and Yu-Xian Li, J. Phys.: Condens. Matter **20**, 465202 (2008).

[16] Bjorn Kubala and Jurgen Konig, Phys. Rev. B , **65**, 245301 (2002).

[17] D. Urban and J. Konig, Phys. Rev. B **79**, 165319 (2009).

[18] G.-B. Zhang, S.-J. Wang, and L. Li, Phys. Rev. B **74**, 085106 (2006).

[19] B. Dong, X. L. Lei, and N. J. M. Horing, J. App. Phys. **104**, 033532 (2008).

[20] L. Qin and Y. Guo, J. Phys.: Condens. Matter **20**, 365206 (2008).

[21] F. Bodoky, W. Belzig, C. Bruder, Phys. Rev. B **77**, 035302 (2008).

[22] B. Dong, H. L. Cui, and X. L. Lei, Phys. Rev. B **69**, 035324 (2004)

[23] P. Meystre and M. Sargent III, *Elements of Quantum Optics, 3rd Ed.* (Springer-Verlab, Berlin, 1998).

[24] I. Djuric, B. Dong, and H. L. Cui, Journal of Applied Physics **99**, 063710 (2006).

[25] He Bi Sun and G. J. Milburn, Phys. Rev. B **59**, 10748 (1999).

[26] J. R. Petta, A. C. Johnson, J. M. Taylor, E. A. Laird, A. Yacoby, M. D. Lukin, C. M. Marcus, M. P. Hanson, A. C. Gossard, Science **309**, 2180 (2005).

[27] G. Burkard and A. Imamoglu, Phys. Rev. B **74**, 041307(R) (2006).

[28] A. Imamoḡlu, D. D. Awschalom, G. Burkard, D. P. DiVincenzo, D. Loss, M. Sherwin, and A. Small, Phys. Rev. Lett. **83**, 4204 (1999).

[29] O. Gywat, F. Meier, D. Loss, and D. D. Awschalom, Phys. Rev. B **73**, 125336 (2006).

[30] Ivana Djuric and Chris P. Search, Phys. Rev. B **74**, 115327 (2006); I. Djuric, M. Zivkovic, C. P. Search, and G. Recine, Physical Review B **78**, 195316 (2008).

[31] David D. Awschalom and Michael E. Flatte, Nature Physics, **3**, 153 (2007).

[32] Y. Ohno, D. K. Young, B. Beschoten, F. Matsukura, H. Ohno, and D. D. Awschalom, Nature, **402**, 790 (1999).

[33] X. Jiang, R. Wang, R. M. Shelby, R. M. Macfarlane, S. R. Bank, J. S. Harris, and S. S. P. Parkin, Phys. Rev. Lett. **94**, 056601 (2005).

[34] D. Loss and E.V. Sukhorukov, Physical Review Letters **84**, 1035-1038 (2000).

## Appendix A: Current Operators

Current operators $\hat{\Gamma}_{L(R)\sigma}$ are given by $33 \times 33$ sparse matrices with all of the elements $\Gamma_{L(R)\sigma}(i,j)$ equal to zero except the following:

The left spin-up current operator $\hat{\Gamma}_{L\uparrow}$:

$$
\begin{aligned}
\Gamma_{L\uparrow}(1,2) &= -(1-f_L(E_\uparrow))\Gamma_{L\uparrow} \\
\Gamma_{L\uparrow}(1,4) &= -(1-f_L(E_\uparrow))\Gamma_{L\uparrow} \\
\Gamma_{L\uparrow}(1,6) &= -(1-f_L(E_\uparrow))\Gamma_{L\uparrow}e^{(-i\Phi/2)} \\
\Gamma_{L\uparrow}(1,8) &= -(1-f_L(E_\uparrow))\Gamma_{L\uparrow}e^{(+i\Phi/2)} \\
\Gamma_{L\uparrow}(2,1) &= f_L(E_\uparrow)\Gamma_{L\uparrow} \\
\Gamma_{L\uparrow}(2,10) &= -(1-f_L(E_\uparrow+U))\Gamma_{L\uparrow} \\
\Gamma_{L\uparrow}(3,13) &= -(1-f_L(E_\uparrow+U))\Gamma_{L\uparrow} \\
\Gamma_{L\uparrow}(4,1) &= f_L(E_\uparrow)\Gamma_{L\uparrow} \\
\Gamma_{L\uparrow}(4,10) &= -(1-f_L(E_\uparrow+U))\Gamma_{L\uparrow} \\
\Gamma_{L\uparrow}(5,12) &= -(1-f_L(E_\uparrow+U))\Gamma_{L\uparrow} \\
\Gamma_{L\uparrow}(10,2) &= f_L(E_\uparrow+U)\Gamma_{L\uparrow} \\
\Gamma_{L\uparrow}(10,4) &= f_L(E_\uparrow+U)\Gamma_{L\uparrow} \\
\Gamma_{L\uparrow}(10,6) &= f_L(E_\uparrow+U)\Gamma_{L\uparrow}e^{(-i\Phi/2)} \\
\Gamma_{L\uparrow}(10,8) &= f_L(E_\uparrow+U)\Gamma_{L\uparrow}e^{(i\Phi/2)} \\
\Gamma_{L\uparrow}(12,5) &= f_L(E_\uparrow+U)\Gamma_{L\uparrow} \\
\Gamma_{L\uparrow}(13,3) &= f_L(E_\uparrow+U)\Gamma_{L\uparrow}
\end{aligned}
$$

The left spin-down current operator $\hat{\Gamma}_{L\downarrow}$:

$$
\begin{aligned}
\Gamma_{L\downarrow}(1,3) &= -(1-f_L(E_\downarrow))\Gamma_{L\downarrow} \\
\Gamma_{L\downarrow}(1,5) &= -(1-f_L(E_\downarrow))\Gamma_{L\downarrow} \\
\Gamma_{L\downarrow}(1,7) &= -(1-f_L(E_\downarrow))\Gamma_{L\downarrow}e^{(-i\Phi/2)} \\
\Gamma_{L\downarrow}(1,9) &= -(1-f_L(E_\downarrow))\Gamma_{L\downarrow}e^{(+i\Phi/2)}
\end{aligned}
$$

$$\Gamma_{L\downarrow}(2,12) = -(1 - f_L(E_\downarrow + U))\Gamma_{L\downarrow}$$
$$\Gamma_{L\downarrow}(3,1) = f_L(E_\downarrow)\Gamma_{L\downarrow}$$
$$\Gamma_{L\downarrow}(3,11) = -(1 - f_L(E_\downarrow + U))\Gamma_{L\downarrow}$$
$$\Gamma_{L\downarrow}(4,13) = -(1 - f_L(E_\downarrow + U))\Gamma_{L\downarrow}$$
$$\Gamma_{L\downarrow}(5,1) = f_L(E_\downarrow)\Gamma_{L\downarrow}$$
$$\Gamma_{L\downarrow}(5,11) = -(1 - f_L(E_\downarrow + U))\Gamma_{L\downarrow}$$
$$\Gamma_{L\downarrow}(11,3) = f_L(E_\downarrow + U)\Gamma_{L\downarrow}$$
$$\Gamma_{L\downarrow}(11,5) = f_L(E_\downarrow + U)\Gamma_{L\downarrow}$$
$$\Gamma_{L\downarrow}(11,7) = f_L(E_\downarrow + U)\Gamma_{L\downarrow}e^{(-i\Phi/2)}$$
$$\Gamma_{L\downarrow}(11,9) = f_L(E_\downarrow + U)\Gamma_{L\downarrow}e^{(i\Phi/2)}$$
$$\Gamma_{L\downarrow}(12,2) = f_L(E_\downarrow + U)\Gamma_{L\downarrow}$$
$$\Gamma_{L\downarrow}(13,4) = f_L(E_\downarrow + U)\Gamma_{L\downarrow}$$

The right spin-up current operator $\hat{\Gamma}_{R\uparrow}$:

$$\Gamma_{R\uparrow}(1,2) = (1 - f_R(E_\uparrow))\Gamma_{R\uparrow}$$
$$\Gamma_{R\uparrow}(1,4) = (1 - f_R(E_\uparrow))\Gamma_{R\uparrow}$$
$$\Gamma_{R\uparrow}(1,6) = (1 - f_R(E_\uparrow))\Gamma_{R\uparrow}e^{(+i\Phi/2)}$$
$$\Gamma_{R\uparrow}(1,8) = (1 - f_R(E_\uparrow))\Gamma_{R\uparrow}e^{(-i\Phi/2)}$$
$$\Gamma_{R\uparrow}(2,1) = -f_R(E_\uparrow)\Gamma_{R\uparrow}$$
$$\Gamma_{R\uparrow}(2,10) = (1 - f_R(E_\uparrow + U))\Gamma_{R\uparrow}$$
$$\Gamma_{R\uparrow}(3,13) = (1 - f_R(E_\uparrow + U))\Gamma_{R\uparrow}$$
$$\Gamma_{R\uparrow}(4,1) = -f_R(E_\uparrow)\Gamma_{R\uparrow}$$
$$\Gamma_{R\uparrow}(4,10) = (1 - f_R(E_\uparrow + U))\Gamma_{R\uparrow}$$
$$\Gamma_{R\uparrow}(5,12) = (1 - f_R(E_\uparrow + U))\Gamma_{R\uparrow}$$
$$\Gamma_{R\uparrow}(10,2) = -f_R(E_\uparrow + U)\Gamma_{R\uparrow}$$
$$\Gamma_{R\uparrow}(10,4) = -f_R(E_\uparrow + U)\Gamma_{R\uparrow}$$
$$\Gamma_{R\uparrow}(10,6) = -f_R(E_\uparrow + U)\Gamma_{R\uparrow}e^{(+i\Phi/2)}$$
$$\Gamma_{R\uparrow}(10,8) = -f_R(E_\uparrow + U)\Gamma_{R\uparrow}e^{(-i\Phi/2)}$$
$$\Gamma_{R\uparrow}(12,5) = -f_R(E_\uparrow + U)\Gamma_{R\uparrow}$$
$$\Gamma_{R\uparrow}(13,3) = -f_R(E_\uparrow + U)\Gamma_{R\uparrow}$$

The right spin-down current operator $\hat{\Gamma}_{R\downarrow}$:

$$\Gamma_{R\downarrow}(1,3) = (1 - f_R(E_\downarrow))\Gamma_{R\downarrow}$$
$$\Gamma_{R\downarrow}(1,5) = (1 - f_R(E_\downarrow))\Gamma_{R\downarrow}$$
$$\Gamma_{R\downarrow}(1,7) = (1 - f_R(E_\downarrow))\Gamma_{R\downarrow}e^{(+i\Phi/2)}$$
$$\Gamma_{R\downarrow}(1,9) = (1 - f_R(E_\downarrow))\Gamma_{R\downarrow}e^{(-i\Phi/2)}$$
$$\Gamma_{R\downarrow}(2,12) = (1 - f_R(E_\downarrow + U))\Gamma_{R\downarrow}$$
$$\Gamma_{R\downarrow}(3,1) = -f_R(E_\downarrow)\Gamma_{R\downarrow}$$
$$\Gamma_{R\downarrow}(3,11) = (1 - f_R(E_\downarrow + U))\Gamma_{R\downarrow}$$
$$\Gamma_{R\downarrow}(4,13) = (1 - f_R(E_\downarrow + U))\Gamma_{R\downarrow}$$
$$\Gamma_{R\downarrow}(5,1) = -f_R(E_\downarrow)\Gamma_{R\downarrow}$$
$$\Gamma_{R\downarrow}(5,11) = (1 - f_R(E_\downarrow + U))\Gamma_{R\downarrow}$$
$$\Gamma_{R\downarrow}(11,3) = -f_R(E_\downarrow + U)\Gamma_{R\downarrow}$$
$$\Gamma_{R\downarrow}(11,5) = -f_R(E_\downarrow + U)\Gamma_{R\downarrow}$$

$$\Gamma_{R\downarrow}(11,7) = -f_R(E_\downarrow + U)\Gamma_{R\downarrow}e^{(+i\Phi/2)}$$
$$\Gamma_{R\downarrow}(11,9) = -f_R(E_\downarrow + U)\Gamma_{R\downarrow}e^{(-i\Phi/2)}$$
$$\Gamma_{R\downarrow}(12,2) = -f_R(E_\downarrow + U)\Gamma_{R\downarrow}$$
$$\Gamma_{R\downarrow}(13,4) = -f_R(E_\downarrow + U)\Gamma_{R\downarrow}$$

The density matrix in vector form, which defines the basis for the current operators, is given by:
$$\vec{\rho}^T = [\rho_{0000}, \rho_{\uparrow0,\uparrow0}, \rho_{\downarrow0,\downarrow0}, \rho_{0\uparrow,0\uparrow}, \rho_{0\downarrow,0\downarrow}, \rho_{\uparrow0,0\uparrow}, \rho_{\downarrow0,0\downarrow}, \quad \rho_{0\uparrow,\uparrow0}, \rho_{0\downarrow,\downarrow0}, \rho_{\uparrow\uparrow,\uparrow\uparrow}, \rho_{\downarrow\downarrow,\downarrow\downarrow}, \rho_{\uparrow\downarrow,\uparrow\downarrow}, \rho_{\downarrow\uparrow,\downarrow\uparrow}, \rho_{\uparrow\downarrow,\downarrow\uparrow}, \rho_{\downarrow\uparrow,\uparrow\downarrow},$$
$$\rho_{\uparrow0,\downarrow0}, \rho_{0\uparrow,0\downarrow}, \rho_{0\uparrow,\downarrow0}, \rho_{0\downarrow,\uparrow0}, \rho_{\downarrow0,0\uparrow}, \rho_{0\downarrow,0\uparrow}, \rho_{\uparrow0,0\downarrow}, \quad \rho_{\uparrow\uparrow,\uparrow\downarrow}, \rho_{\uparrow\downarrow,\uparrow\uparrow}, \rho_{\uparrow\uparrow,\downarrow\uparrow}, \rho_{\downarrow\uparrow,\uparrow\uparrow}, \rho_{\uparrow\uparrow,\downarrow\downarrow}, \rho_{\downarrow\downarrow,\uparrow\uparrow}, \rho_{\uparrow\downarrow,\downarrow\downarrow}, \rho_{\downarrow\downarrow,\uparrow\downarrow},$$
$$\rho_{\downarrow\uparrow,\downarrow\downarrow}, \rho_{\downarrow\downarrow,\downarrow\uparrow}].$$

## Appendix B: Matrix M

Matrix $M$ is a $33 \times 33$ sparse matrix with the following non-zero elements $M(i,j)$:

$$M(2,1) = M(4,1) = \alpha_{1\uparrow}, M(3,1) = M(5,1) = \alpha_{1\downarrow}$$
$$M(1,2) = M(1,4) = \beta_{1\uparrow}, M(1,3) = M(1,5) = \beta_{1\downarrow}$$
$$M(8,1) = M(6,1)^* = \alpha_{2\uparrow}, M(9,1) = M(7,1)^* = \alpha_{2\downarrow}$$
$$M(1,6) = M(1,8)^* = \beta_{2\uparrow}, M(1,7) = M(1,9)^* = \beta2\downarrow$$
$$M(10,2) = M(10,4) = M(12,5) = M(13,3) = \tilde{\alpha}_{1\uparrow}$$
$$M(11,3) = M(11,5) = M(12,2) = M(13,4) = \tilde{\alpha}_{1\downarrow}$$
$$M(2,10) = M(3,13) = M(4,10) = M(5,12) = -\frac{1}{2}M(10,10) = \tilde{\beta}_{1\uparrow}$$
$$M(2,12) = M(3,11) = M(4,13) = M(5,11) = -\frac{1}{2}M(11,11) = \tilde{\beta}_{1\downarrow}$$
$$M(10,6) = M(10,8)^* = M(14,9)^* = M(15,7) = \tilde{\alpha}_{2\uparrow}$$
$$M(11,7) = M(11,9)^* = M(14,6) = M(15,8)^* = \tilde{\alpha}_{2\downarrow}$$
$$M(6,10)^* = M(7,14)^* = M(8,10) = M(9,15) = \tilde{\beta}_{2\uparrow}$$
$$M(6,15)^* = M(7,11)^* = M(8,14) = M(9,11) = \tilde{\beta}_{2\downarrow}$$
$$M(2,2) = M(4,4) = M(6,6)^* = M(8,8) = -(\beta_{1\uparrow} + \tilde{\alpha}_{1\uparrow} + \tilde{\alpha}_{1\downarrow})$$
$$M(3,3) = M(5,5) = M(7,7)^* = M(9,9) = -(\beta_{1\downarrow} + \tilde{\alpha}_{1\uparrow} + \tilde{\alpha}_{1\downarrow})$$
$$M(2,6) = M(2,8)^* = M(4,6) = M(4,8)^* = M(6,2)^* = M(6,4)^* = M(8,2) = M(8,4) = -\frac{1}{2}(\beta_{2\uparrow} + \tilde{\alpha}_{2\uparrow})$$
$$M(3,7) = M(3,9)^* = M(5,7) = M(5,9)^* = M(7,3)^* = M(7,5)^* = M(9,3) = M(9,5) = -\frac{1}{2}(\beta_{2\downarrow} + \tilde{\alpha}_{2\downarrow})$$
$$M(1,1) = -2(\alpha_{1\uparrow} + \alpha_{1\downarrow})$$
$$M(12,12) = M(13,13) = -(\tilde{\beta}_{1\uparrow} + \tilde{\beta}_{1\downarrow})$$
$$M(14,14) = M(15,15)^* = -(\tilde{\beta}_{2\uparrow}^* + \tilde{\beta}_{2\downarrow})$$
$$M(16,16) = M(20,20)^* = M(17,17) = M(21,21)^* = M(18,18) = M(22,22)^* = M(19,19)^* = M(23,23)$$
$$= \frac{1}{2}M(28,28) = \frac{1}{2}M(29,29)^* = -2i\Omega$$
$$M(24,24) = M(25,25)^* = M(26,26) = M(27,27)^* = -i(2\Omega + \frac{J_z}{2})$$
$$M(30,30) = M(31,31)^* = M(32,32) = M(33,33)^* = -i(2\Omega - \frac{J_z}{2})$$
$$M(12,24) = -M(12,15) = M(13,15) = -M(13,14) = M(14,12) = -M(14,13) = M(15,13) = -M(15,12)$$
$$= M(24,26) = -M(25,27) = M(26,24) = -M(27,25) = -M(30,32) = M(31,33)$$
$$= -M(32,30) = M(33,31) = iJ_n$$
$$M(2,16) = -M(2,20) = -M(3,16) = M(3,20) = -M(6,22) = -M(7,23) = M(8,18) = M(9,19)$$

$$
\begin{aligned}
&= M(10,26) = -M(10,27) = M(11,31) = -M(11,30) = M(12,30) = -M(12,31) \\
&= M(13,27) = -M(13,26) = M(14,25) = -M(14,33) = M(15,32) = -M(15,24) = M(16,2) \\
&= -M(16,3) = -M(20,2) = M(20,3) = M(18,8) = -M(22,6) = M(19,9) = -M(23,7) \\
&= M(24,28) = -M(24,15) = M(25,14) = -M(25,29) = M(26,10) = -M(26,13) = M(27,13) \\
&= -M(27,10) = M(28,24) = -M(28,32) = M(29,33) = -M(29,25) = M(30,12) = -M(30,11) \\
&= M(31,11) = -M(31,12) = M(32,15) - M(32,28) = M(33,29) = -M(33,14) = iR_1 \\
M(4,17) \quad &= -M(4,21) = -M(5,17) = M(5,21) = M(6,23) = M(7,22) = -M(8,19) = -M(9,18) \\
&= M(10,24) = -M(10,25) = M(11,33) = -M(11,32) = M(12,25) = -M(12,24) = M(13,32) \\
&= -M(13,33) = M(14,30) = -M(14,26) = M(15,27) = -M(15,31) = M(17,4) = -M(17,5) \\
&= -M(21,4) = M(21,5) = -M(18,9) = M(22,7) = -M(19,8) = M(23,6) = M(24,10) \\
&= -M(24,12) = M(25,12) = -M(25,10) = M(26,28) = -M(26,14) = M(27,15) = -M(27,29) \\
&= M(28,26) = -M(28,30) = M(29,31) = -M(29,27) = M(30,14) = -M(30,28) = M(31,29) \\
&= -M(31,15) = M(32,13) = -M(32,11) = M(33,11) = -M(33,13) = iR_2
\end{aligned}
$$